



## Using the Maximum Effective Moment Criterion to Interpret Quartz <c>-Fabric Patterns

ZHENG Yadong, ZHANG Jinjiang and ZHANG Bo\*

The Key Laboratory of Orogenic Belts and Crustal Evolution, School of Earth and Space Sciences, Peking University, Beijing 100871, China

**Abstract:** The Maximum Effective Moment (MEM) criterion predicts that the initial orientation of ductile shear zones and shear bands is  $\sim 55^\circ$  relative to the maximum principal stress axis ( $\sigma_1$ ) and that the kinematic vorticity number ( $W_k$ ) is  $\sim 0.94$ . These preferred orientations should be reflected in the pattern of quartz <c>-fabrics in shear zones and shear bands. Common quartz <c>-fabrics in plane strain can be divided into low-temperature (L) and high-temperature (H) fabrics, with each group showing three patterns. A steady flow with a constant value of  $W_k \approx 0.94$  gives rise to L-1 and H-1 patterns, which are commonly characterized by a single <c> axis girdle normal to the shear zone and a single <c>-point maximum parallel to the shear zone. Once the conjugate set develops, L-1 and H-1 have opening angles of  $\sim 70^\circ$  and  $\sim 110^\circ$ , respectively. L-2 and H-2 are asymmetric patterns associated with variable deformation partitioning and vorticity values of  $0 < W_k < 0.94$ . In contrast, L-3 and H-3 are symmetric patterns associated with 100% deformation partitioning and  $W_k = 0$ . The opening angle in quartz <c>-fabrics is implicitly linked to the temperature during deformation. The opening angle is  $\sim 70^\circ$  at low temperature and  $\sim 110^\circ$  at high temperature. However, a linear correction between the opening angle and the temperature cannot be established. During deformation partitioning, synthetic shear bands form earlier than antithetic bands and are more easily developed. This may result in opening angles of  $< 70^\circ$  for low-temperature fabrics and of  $> 110^\circ$  for high-temperature fabrics. The following criteria can be used to recognize reworked shear zones that have experienced multiple orogenic phases and changes in the stress state: 1) the initial  $W_k$  is larger or smaller than  $\sim 0.94$ ; 2) the change in  $W_k$  is abrupt, rather than progressive; 3) inconsistent shear senses are inferred for the different phases of deformation; and 4) a negative value of  $W_k$  is found in reworked shear zones.

**Key words:** deformation localization, deformation partitioning, shear bands, vorticity  $W_k$ , quartz CPO patterns

Citation: Zhang et al., 2019. Using the Maximum Effective Moment Criterion to Interpret Quartz <c>-Fabric Patterns. Acta Geologica Sinica (English Edition), 93(4): 799–809. DOI: 10.1111/1755-6724.13855

### 1 Introduction

Forty years ago, the metallurgical term “shear bands” was first used to describe oblique, partially penetrative, intrafolial, internal shears in mylonites (White, 1979) (Fig. 1). Three unresolved problems arise from the recognition of these structural features. First, it is unclear why the angle between conjugate shear bands is obtuse rather than acute, as predicted by the Mohr–Coulomb failure criterion. Ramsay (1980) suggested that progressive contraction could be responsible for increasing the angle between conjugate structures, but such a process cannot explain spaced shear bands that truncate a penetrative mylonitic foliation. Accordingly, the obtuse angle between conjugate shear bands is likely the original angle. Second, the maximum principal stress referred from the conjugate shear bands is normal to the shear boundaries rather than  $45^\circ$  predicted by the simple shear theory prevailing at that time or any other oblique angles by general shear theory nowadays. What a process changed the stress state from one to another? Third, the observation that synthetic shear bands ( $C'$ ) are so well developed raises the question as to

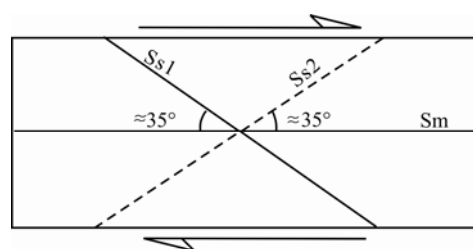


Fig. 1. Conjugate shear bands in mylonites (after White, 1979). Sm, mylonitic foliation; Ss1, synthetic shear bands; Ss2, antithetic shear bands.

why conjugate shear bands are asymmetric.

The Maximum Effective Moment (MEM) criterion was proposed by Zheng et al. (2004) to address the above problems. An increasing number of observations, both in nature and from experiments, have confirmed the accuracy of the MEM criterion (Fig. 2a–c). However, the criterion has so far not been applied in petrofabric analysis. The aim of this paper is tentatively to interpret crystallographic preferred orientation patterns (quartz <c>-fabric patterns) in the context of the MEM criterion.

\* Corresponding author. E-mail: geozhangbo@pku.edu.cn

## 2 The MEM Criterion for Localization

Based on the analysis of conjugate shear bands and kinkbands, the following equation was formulated (Zheng et al., 2004) to describe the failure of a shear band with a certain width, for stresses applied on the boundaries of a finite unit cube (Fig. 2a):

$$M_{eff} = \pm \frac{1}{2} (\sigma_1 - \sigma_3) L \sin 2\alpha \cos \alpha \quad (1)$$

Where  $M_{eff}$  is effective moment;  $(\sigma_1 - \sigma_3)$  is the yield strength of the deformed material;  $\alpha$  is the angle between  $\sigma_1$  and the shear bands; and  $L$  is a unit length (Fig. 2a-b).

The mathematical expression of the MEM criterion implies that once the differential stress reaches the yielding point of the material (for certain temperature, confining pressure, fluid pressure, and strain rate conditions), conjugate shear zones form at an angle of  $\sim 55^\circ$  relative to  $\sigma_1$ . The occurrence of pairs of conjugate MEM orientations follows the theorem of conjugate stress in the mechanics of materials, which states that shear stresses with opposite sense must have an equivalent absolute value (otherwise the finite cube would be unbalanced and rotate).

The shaded area in Figure 2c is the field of available data from natural and experimental observations. These observations were made at different scales in homogeneous, inhomogeneous, isotropic, and anisotropic materials. The fact that all data plot in a relatively narrow field may suggest that the MEM criterion is widely applicable to multiscale structural features in various materials.

Deformation does occur in the whole area of the considered unit (Fig. 2a, b) but is limited to pairs of kink bands, shear bands, or shear zone sets. Incipient shear zones may occur where the wall-rocks remain undeformed, and shear zones may decrease in thickness and increase in length. This implies that the shear zone boundaries are parallel to the extensional apophysis  $AP_1$  (see Section 3). Shear zones can become narrower in both extensional and compressional tectonic settings, for example, in association with low-angle normal faults, high-angle reverse faults, and wide-open V-shaped conjugate strike-slip faults (Zheng et al., 2011, 2015). For shear zones to become broader, a change in the stress state after

formation is required, most likely caused by orogenic reworking.

## 3 Geometry, Kinematics, and Mechanics of Steady Flows and Ductile Shear Zones

Previous studies have demonstrated that ductile shear zones in nature are characterized by a range of vorticity numbers (Xypolias, 2010, and references therein). The different methods used to derive vorticity numbers have considered continuous and homogeneous deformation. For the simplified case of a two-dimensional ductile shear zone without volume loss, Bobyarchick (1986) and Passchier (1986) defined the kinematic vorticity number ( $W_k$ ) as:

$$W_k = \cos \nu, \quad (2)$$

where  $\nu$  is the angle between the flow apophyses, which can range from  $0^\circ$  to  $90^\circ$ .

An alternative definition can be given in stress terms (Weijermars, 1991, 1998):

$$W_k = \sin 2x, \quad (3)$$

where  $x$  is the angle between  $s_1$  and the normal to the shear boundary. This angle can range from  $0^\circ$  to  $45^\circ$ .

The definitions in Equations 2 and 3 are equivalent, with both strictly valid only in two-dimensional flows (e.g., Tikoff and Fossen, 1995; Xypolias, 2010).  $W_k$  is a measure of non-coaxiality during deformation, with simple shear and pure shear being the two end members whereby  $W_k = 1$  and  $W_k = 0$ , respectively (e.g., Weijermars, 1991; Xypolias, 2010).

The apparent variation in the calculated vorticity of ductile shear zones in nature could misleadingly imply that shear zones develop at random orientations relative to  $s_1$ . According to the MEM criterion, ductile shear zones nucleate  $55^\circ$  relative to  $s_1$  and  $ISA_3$  (the minimum instantaneous stretching axis), and  $135^\circ$  relative to  $s_3$  and  $ISA_1$  (the maximum instantaneous stretching axis). In plane strain, these shear boundaries correspond to  $W_k = 0.94$ . This prediction is supported by observations that the angle  $\beta$  between S- and C- foliations is commonly lower than  $35^\circ$  (e.g., Law et al., 1994), and the angle between quartz ribbons and the grain shape fabric is lower than  $42^\circ$  (e.g., Passchier and Trouw, 2005; Little et al., 2013; Sarkarinejad et al., 2015). Numerical models used to check the reliability of the widely used Porphyroclast Hyperbolic Distribution have shown that reported vorticity

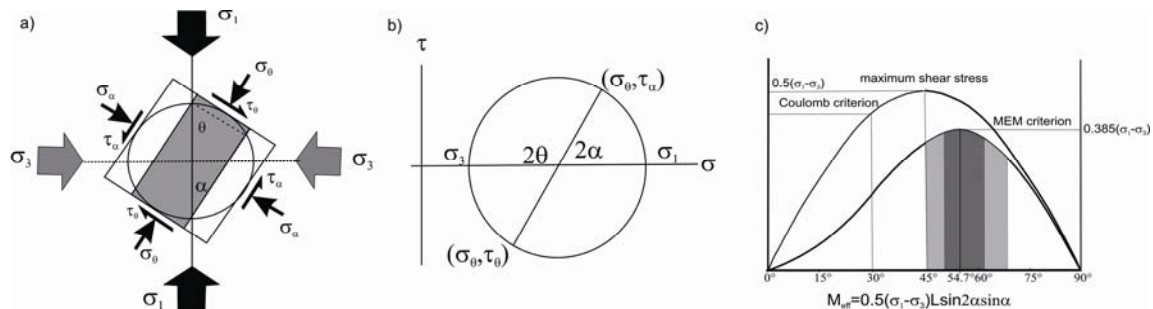


Fig. 2. Derivation of the MEM criterion (after Zheng et al., 2004).

(a) Stress field applied on a finite cubic unit; (b) Mohr circle showing the state of stress in the finite unit cube; (c) Mathematical and graphical expressions of the MEM criterion.  $\sigma_1$ - $\sigma_3$  is the yield strength,  $L$  is the unit length, and  $\alpha$  is the angle between  $\sigma_1$  and the shear bands/zones. All data from field and laboratory observations are plotted in the shaded area, with the dark area indicating experimental data from Gomez-Rivas and Griera (2012).

numbers in the range of 0.50–0.85 in natural shear zones were likely associated with a flow regime close to simple shear (Li and Jiang, 2010, and reference therein). In other words, most shear zones in nature have likely formed at an orientation of  $55^\circ$  relative to  $s_1$ .

The development of a penetrative S-foliation is the result of quasi-homogeneous deformation involving a loading rate lower than the relaxation rate. The spaced C-planes result from deformation localization associated with a loading rate higher than the relaxation rate. The coexistence of S- and C-foliations in mylonites, as suggested by Hubert-Ferrari (2003) and Gomez-Rivas (2008), can be regarded as a competing process between an external loading rate and the rate of viscous relaxation. If the former is higher than the latter, the differential stress increases until the yielding point is reached, thus producing ductile shear features that subsequently propagate. Alternatively, the imposed stresses will relax if the viscous relaxation rate is higher than the rate of external loading, leading to the development of a penetrative S-foliation. C/S fabrics reflect the competition of these two deformation mechanisms and imply that each set of foliations is developed in a critical state of dynamic balance. The situation is similar to the transition from a Lüders band to the Portevin–Le Chatelier effect, which describes a serrated stress-strain curve (or jerk flow) in inhomogeneous plastic deformation (Ananthakrishna, 2007). This effect has been attributed to the competition between diffusing solutes pinning dislocations, and dislocation breaking free of this stoppage (Abbadi et al., 2002), which is equivalent to the competition between deformation localization and homogeneous deformation. Therefore, the predicted  $W_k$  of 0.94 also implies that the corresponding angle  $\nu$  between the two apophyses of flow

is  $20^\circ$ .

Shear zones with C-surfaces are parallel to the extensional apophysis ( $AP_1$ ), with the conjugate set being expected to form normal to the contractional apophysis ( $AP_2$ ). This orientation is  $\sim 20^\circ$  relative to the normal of  $AP_1$  (Fig. 3).

Simpson and De Paor (1993) suggested that conjugate shear bands initiate parallel to the orientations of maximum (angular) shear strain. The two orientations are parallel to the bisectors of the acute (AB) and the obtuse (OB) apophyses, respectively. Although these predictions are widely accepted (e.g., Kurd and Northrup, 2008; Sullivan, 2009; Xypolias, 2010; Gillam et al., 2014), they contradict experimental data and field observations, which show a conjugate angle of  $\sim 110^\circ$  rather than  $\sim 90^\circ$  (Fig. 1; Zheng, et al., 2004, 2009, 2011, 2014, 2015).

A case with two major synthetic shear band sets and one antithetic set has been discussed by Kurd and Northrup (2008) (Fig. 4a). In this analysis, the second set was regarded as the acute bisector, thus meeting the  $90^\circ$  angle predicted by the maximum-shear-strain-rate presumption. However, the angle between the first synthetic set and the antithetic set is  $\sim 114^\circ$ , and the angle between the second set and the normal to  $AP_1$  is  $55^\circ$ . Both angles are in the range predicted by the MEM criterion (Fig. 4b).

The mylonitic foliation is, in fact, commonly truncated by synthetic and antithetic shear bands at different cut-off angles, with the cut-off angles of the synthetic shear bands ( $15^\circ$ – $35^\circ$ ) being lower than the cut-off angles ( $35^\circ$ – $55^\circ$ ) of the antithetic shear bands (Fig. 3a). The conjugate angle, however, is relatively consistent ( $\sim 110^\circ$ ). The mylonitic foliation is parallel to the shear zone boundary in the central section of the Alpine Fault mylonite zone, and the mean cut-off angle of the synthetic shear bands is  $\sim 30^\circ$ .

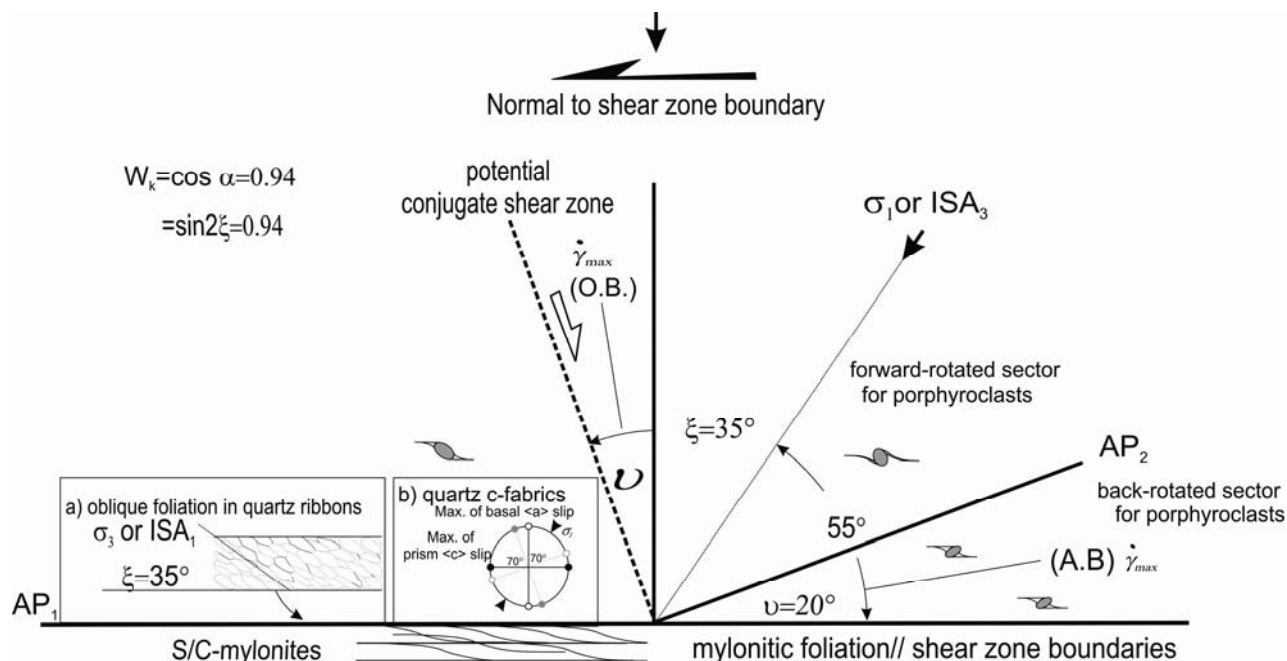


Fig. 3. Geometry, kinematics, and mechanics of a steady ductile shear zone.

$AP_1$  and  $AP_2$  are the extensional and shortening apophyses, respectively.  $\nu$  is the angle between the two apophyses,  $\sigma_1$  is the maximum principal stress,  $ISA_3$  is the minimum instantaneous stretching axis,  $x$  is the angle between  $\sigma_1$  (or  $ISA_3$ ) and the normal to  $AP_1$ , and  $\dot{\gamma}$  is the maximum shear strain rate (Simpson and De Paor, 1993). (a) Oblique foliation in quartz ribbons parallel to  $\sigma_3$  and  $ISA_1$ ; (b) quartz c-axis fabrics at low and high temperature. Note that in steady flows, conjugate shear zones form in the MEM orientations and not in the orientations of A.B and O.B..

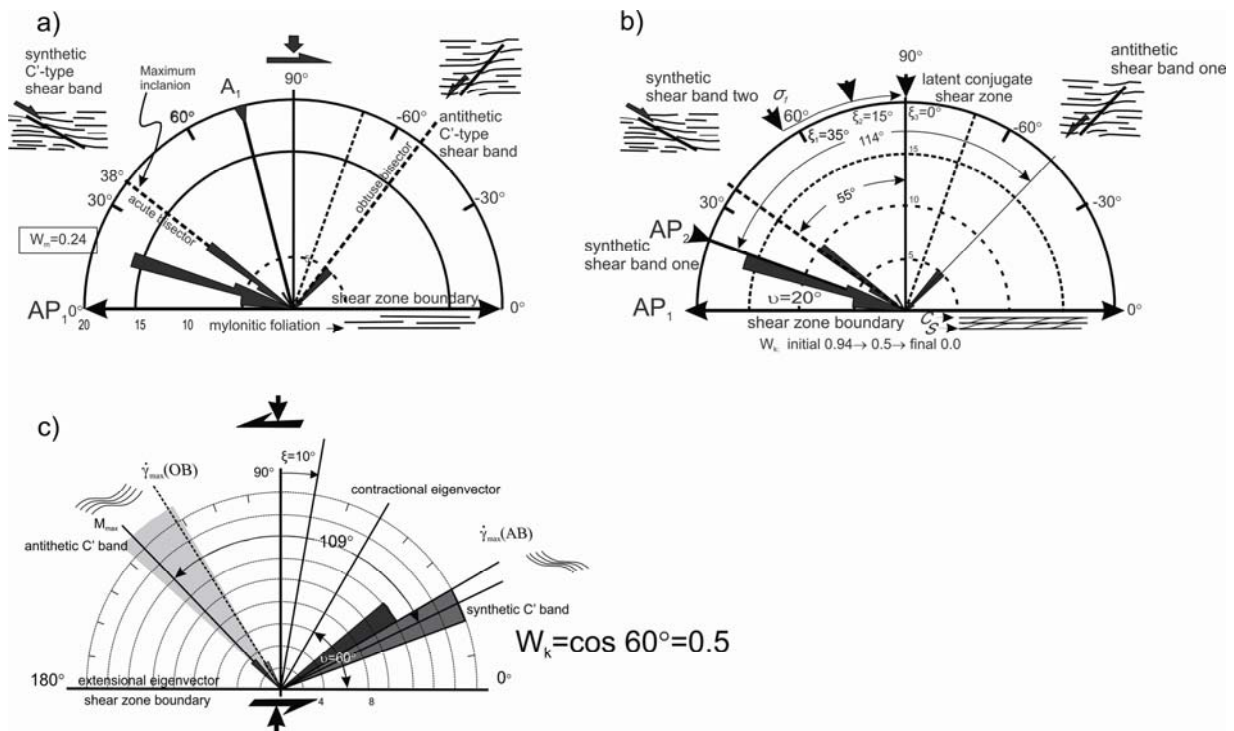


Fig. 4. Different interpretations for development of shear bands.

(a) Popular explanation of orientations of shear bands in flow field (Kurd and Northrup, 2008; Xypolias, 2010); (b) explanation of orientations of shear bands in terms of MEM criterion (Zheng et al., 2009); (c) Gillam et al. (2014) regarded the 30°-angle between the synthetic bands (C') and the shear boundary as AB-line, corresponding  $W_k=0.5$ . If the hypothesis that shear bands along the maximum shear strain rate directions were correct, the expected antithetic shear bands would be parallel to the OB-line and normal to the synthetic ones. However, the observations do not support the presumption. According to the MEM-criterion,  $W_k=\sin 20^\circ=0.34$

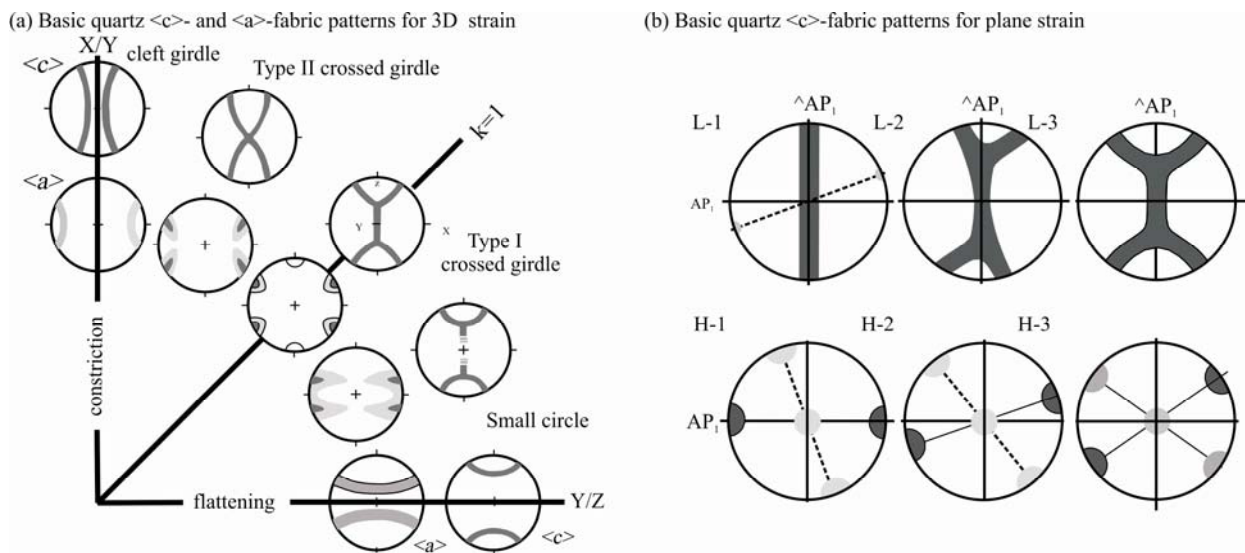


Fig. 5. The relationships between quartz CPO patterns and strain types.

(a) Flinn diagram showing quartz <c>-fabric geometries (Lister and Hobbs, 1980) and corresponding <a>-axis fabric geometries (Schmid and Casey, 1986). X, Y, and Z are the maximum, intermediate, and minimum axes of the finite strain ellipsoid. The line  $k = 1$  represents plane strain (adapted from Sullivan and Beane, 2010); (b) quartz <c>-fabric patterns for plane strain (Passchier and Trouw, 2005).

The antithetic shear bands have larger cut-off angles, typically  $\sim 40^\circ$ . Gillam et al. (2014) regarded the 30° angle between the synthetic bands (C') and the shear boundary as the AB line. If the hypothesis that shear bands along the maximum angular shear strain rate directions was correct, the expected antithetic shear bands would be parallel to

the OB line and normal to the synthetic shear bands. However, the observations do not support the presumption (Fig. 4c). Antithetic shear bands are oriented in the 139° direction, and the conjugate angle is 109°, which is considerably larger than 90°. Alternatively, Zheng et al. (2004) suggested that conjugate shear bands more likely



developed parallel to the MEM orientations, with the conjugate angle of  $109^\circ$  being predicted by the MEM criterion.

#### 4 Common Quartz *c*-Fabric Patterns

Basic quartz *c*-fabric patterns (Fig. 3b; 5a, b) have been predicted from numerical simulations of plastic deformation, based on the Taylor–Bishop–Hill model for slip-system activation (Lister and Hobbs, 1980). A variety of fabrics from both naturally and experimentally deformed samples support the results of numerical simulations (Tullis, 1977; Compton, 1980; Law et al., 1984; Price, 1985; Schmid and Casey, 1986; Law, 1986). The modeling result (Lister and Hobbs, 1980) shows that the central segment of quartz *c*-axis fabrics is orthogonal to the flow plane, indicating a basal *a* slip. Based on this relationship, the finite-strain/quartz *c*-axis-fabric ( $R_{xz}/\beta$ ) method has been proposed to estimate the value of  $W_k$  (Wallis, 1995) (Fig. 6b, c).

For simplicity, the description here is restricted to plane-strain deformation, but patterns forming at high temperature are considered. At low temperature, the central segment of quartz *c*-axis fabrics is orthogonal to the shear plane, whereas at high temperature, the point maxima of quartz *c*-fabrics are parallel to the *c*-slip surfaces. Therefore, the former can be regarded as the normal direction to the boundary of the shear zone and the latter as the direction parallel to the shear zone. If C-surfaces in C/S fabrics (Lister and Snoke, 1984) represent the orientation parallel to the shear zone (e.g., Passchier and Trouw, 2005; Xypolias, 2010), the most common quartz *c*-axis patterns shown in XZ-Cartesian coordinates will be associated with an anti-shear sense rotated by *b* (Fig. 5b). Using L and H for low and high temperature, respectively, the following patterns are recognized: 1) L-1 single girdle perpendicular to the shear zone boundary ( $AP_1$ ); 2) L-2 asymmetric crossed girdle normal to  $AP_1$ ; 3) L-3 symmetric crossed girdle normal to  $AP_1$ ; 4) H-1 single-point maximum on the  $AP_1$  perimeter; 5) H-2 asymmetric double-point maxima on the  $AP_1$  perimeter; and 6) H-3 symmetric double-point maxima on the  $AP_1$  perimeter. L-1 and H-1 represent steady flows without deformation partitioning, L-3 and H-3 represent 100% deformation partitioning, and L-2 and H-2 belong to another percentage of deformation partitioning. Representative cases are shown in Figure 6a and c.

##### 4.1 Type L-1

This type of fabric is characterized by a single *c* axis girdle, composed of slip systems (basal *a*, rhomb *a*, and prism *a*) that are normal to the shear zone boundary (Figs 5b and 6a). The opening angle is commonly zero, as crossed girdles are not developed. However, as shown in Figures 5 and 6a, there is a potential conjugate shear zone in another MEM direction, with its normal oriented  $\sim 70^\circ$  antithetically relative to the single girdle. Once this conjugate shear zone forms, the opening angle is  $\sim 70^\circ$  (Fig. 5b and wys-153 and 154 in Fig. 6). The predicted orientation of  $\sigma_1$  (or  $ISA_3$ ) is  $55^\circ$  synthetically relative to the shear zone boundaries ( $AP_1$ ), and the corresponding

$W_k$  is  $\sim 0.94$  in plane strain (Fig. 3). As the shear zone initiated in one of the MEM directions, the  $\beta$ -angle between the S- and C- planes likely formed as  $\sim 35^\circ$ . For steady flows, the flow apophyses with respect to the shear zone boundary remain constant throughout the deformation history. This means that the  $W_k$  remains constant despite the decrease in  $\beta$  during deformation (Fig. 6b). A number of examples from shear zones in nature and the expected deformation paths are shown in Figure 6a and b, respectively.

##### 4.2 Type L-2

This pattern is characterized by an asymmetric crossed girdle, which is composed of slip systems (basal *a* slip, rhomb *a* slip, and prism *a*) with an opening angle of  $< 70^\circ$  (Fig. 6a). Although the central girdle remains normal to the shear zone boundaries ( $AP_1$ ), two point maxima branch as front maximum and trail maximum. The occurrence of crossed girdle or trailed maximum implies a two-stage deformation (Lister, 1977; Lister et al., 1978; Lister and Hobbs, 1980). The central girdle records the first stage of deformation with  $W_k=0.94$ , and the two point maxima represent the second stage of deformation history with the vorticity value being  $0 < W_k < 0.94$ . The two point maxima imply that deformation partitioning has occurred with the front maximum representing the synthetic shear bands, which progressively changed their position from the original orientation of the C-plane because of the change in the stress state. Field observations show that synthetic shear bands are typically oriented  $15^\circ$ – $35^\circ$  relative to the shear zone boundaries (e.g., Berthé et al., 1979; Platt and Vissers, 1980), and numerical studies show that shear bands are non-rotating and shallowly inclined ( $< 30^\circ$ ) with respect to the flow plane (e.g., Grasemann et al., 2003). As shown in Figure 4a, orientations of synthetic shear bands range from nearly parallel to the shear zone boundary (or C-planes) to  $35^\circ$  relative to it. This confirms that the synthetic shear bands resulted from deformation partitioning at different levels. The fact that spaces between C-planes are much narrower relative to the spaces between shear bands implies that the early stage of deformation was more penetrative and occurred at a higher temperature. The later low-temperature deformation was likely confined to the basal *a*-slip system, with the central segment of the crystal fabric remaining undeformed. As such, shear bands form when the mylonitic foliation is already established, thus recording late syn-mylonitization or early post-mylonitization deformation (e.g., Passchier and Trouw, 2005; Xypolias, 2010). In a strict sense, once the shear bands form, there is no flow but only deformation localization. This is supported by numerical studies, which confirm that shear bands are of non-rotating features. Here, it is suggested that the central girdle forms at a medium temperature and remains frozen in the mylonitic foliations as the temperature drops, whereas the basal *a*-slip system (associated with the shear bands) remains active and forms the front maximum. In cases that the basal *a*-slip also occurs along the S-foliation or the conjugate shear bands, a trail maximum may form an angle of  $< 70^\circ$  relative to the synthetic shear bands. Once

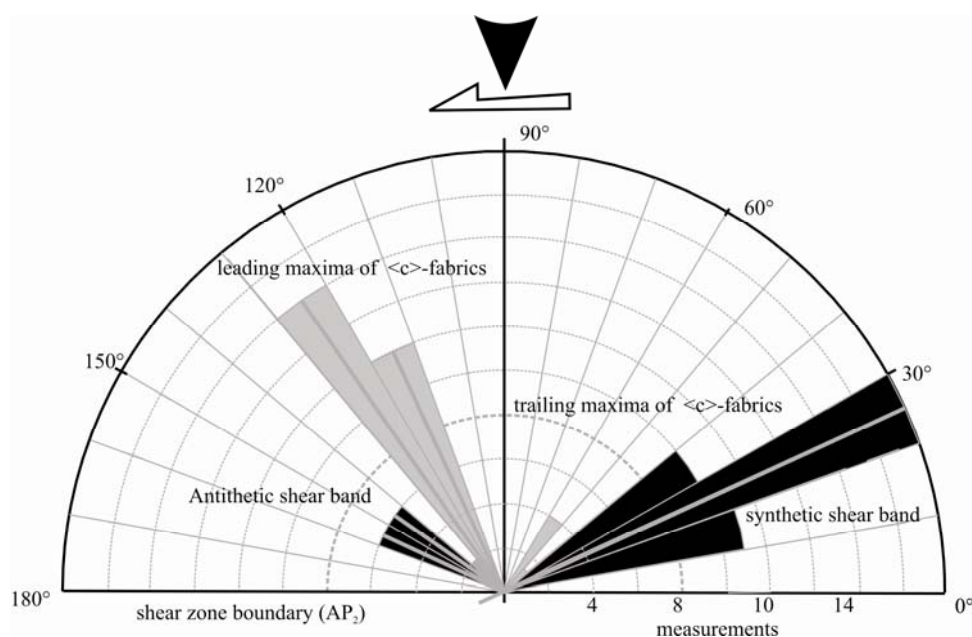


Fig. 7. Rose diagram showing the front and trailing maxima of low-temperature  $\langle c \rangle$ -fabrics. The two orientations are normal to synthetic and antithetic shear bands, respectively. The case shown involves  $\sim 100\%$  deformation partitioning (data from Law et al., 2013).

the shear bands develop,  $W_k$  can be estimated from the branch-out angle of the front maximum, which represents the normal to the basal  $\langle a \rangle$  slip along the synthetic shear bands. The orientation of  $\sigma_1$  (or  $ISA_3$ ) is  $35^\circ$  backward relative to the front maximum. Depending on the degree of deformation partitioning, the trail maximum may either represent the normal to the S-foliation (for a trail maximum in the range of  $0^\circ$ – $35^\circ$ ) or the normal to the antithetic shear bands, which ranges from  $20^\circ$  to  $35^\circ$ .

Central girdles that appear oblique to the shear plane likely rotated synthetically towards the shear direction with increasing strain and dynamic recrystallization (e.g., Heilbronner and Tullis, 2006). This deformation likely occurred at comparatively high temperature.

#### 4.3 Type L-3

This pattern shows a central girdle that remains normal to the shear zone boundaries ( $AP_1$ ), and two symmetric point maxima  $\sim 35^\circ$  from the central girdle. This means that a pair of  $\langle c \rangle$ -fabrics represents normals to the conjugate basal  $\langle a \rangle$  slip sets with an angle of  $\sim 110^\circ$  between them. This pattern is identical to the pattern shown in Figures 1 and 7, suggesting that the two  $\langle c \rangle$  point maxima are controlled by the conjugate shear bands and hence by the MEM orientations. The orientation of  $\sigma_1$  ( $ISA_3$ ), deduced from the obtuse bisector between the two point maxima, indicates that the value of  $W_k$  is zero, thus implicating a 100% deformation partitioning (Tikoff and Teyssier, 1994; Teyssier et al., 1995). In such a stress state, slip systems parallel to the shear zone boundaries cannot slip, and the central girdle segment is a historical record as the normal to the shear zone.

#### 4.4 Type H-1

This pattern shows a single-point c-maximum on the

perimeter at  $AP_1$ , associated with the prism  $\langle c \rangle$ -slip system. The orientation is parallel to the shear zone boundaries ( $AP_1$ ) and the mylonitic C-plane. Opening angles are absent, as the potential conjugate maximum is commonly annihilated by the major shear zone (GPS-126-1-G, PNG-09-024b, and PNG-08-037c in Fig. 6a).

The predicted orientation of  $\sigma_1$  (or  $ISA_3$ ) is  $55^\circ$  synthetically relative to the shear zone boundaries ( $AP_1$ ), corresponding to  $W_k=0.94$  in plane strain. As the shear zone initiated in one the MEM directions, the initial  $\beta$ -angle between S- and C-planes is  $\sim 35^\circ$ . For steady-state flow, there is no change in the orientation of the flow apophyses relative to the shear zone boundary throughout the history of deformation. This means that  $W_k$  remains constant as  $\beta$  decreases. A number of examples from shear zones in nature and the expected deformation paths are shown in Figure 6a and b, respectively.

As shown in Figure 3, a potential conjugate shear zone forms in the other MEM direction, at an angle of  $\sim 110^\circ$  synthetically relative to the main shear zone and  $20^\circ$  relative to the normal to  $AP_1$ . Accordingly, a point maximum caused by the prism  $\langle c \rangle$ -slip system may appear in this orientation. This point maximum tends to be mixed with the basal  $\langle a \rangle$ -slip system at low temperature.

Deformation bands have been reported in high-temperature gneisses from the D'Entrecasteaux Islands, Papua New Guinea (Little et al., 2011, 2013). Abundant conjugate extensional shear bands in hornblende-bearing quartzofeldspathic gneisses from the carapace zones, as well as deformation bands in quartz from the core-zone gneisses, have been observed. These structures typically occur in pairs separated by an angle of  $\sim 70^\circ$  or  $\sim 110^\circ$  (e.g., PNG-06-034a in Fig. 6a and Fig. 8). Misorientation profiles reveal small ( $< 2^\circ$ ) rotations of the crystal lattice across the boundaries of deformation bands, indicating

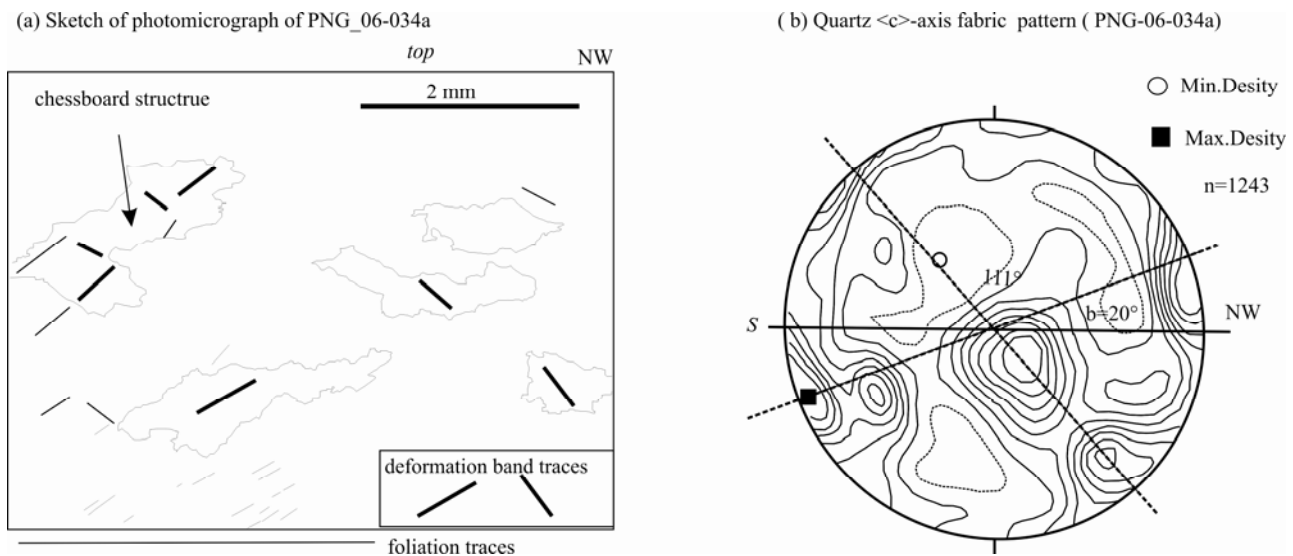


Fig. 8. Concordance between deformation bands, oblique grain shape fabrics, and  $\langle c \rangle$ -axis fabrics (after Little et al., 2013, sample PNG-06-034a).

(a) The original explanation (Little et al., 2013), involving activity in high temperature of both the basal  $\langle a \rangle$ - and prism  $\langle c \rangle$ -slip in quartz. The prismatic deformation bands are subparallel to the  $\langle c \rangle$ -axis maximum, and the basal deformation bands are perpendicular to it. These two types yield a quasi-orthogonal pattern of deformation bands. (b) An alternative explanation in which the angle between the two maxima and the two deformation bands is  $\sim 70^\circ$  or  $110^\circ$  (rather than  $90^\circ$ ). Therefore, they are conjugate prism  $\langle c \rangle$ -slip systems. The parallelism between the orientation of deformation bands and grain shape fabrics in quartz likely resulted from deformation partitioning at the microscale.

that these structures have a similar origin as shear bands controlled by the MEM criterion. However, this quasi-orthogonal pattern is explained by the combination of activity along the basal  $\langle a \rangle$ - and prism  $\langle c \rangle$ -slip systems in quartz at high temperature, with the prismatic deformation bands being subparallel to the  $\langle c \rangle$ -axis and the basal deformation bands perpendicular to it. These two types of CPO patterns seem to yield a quasi-orthogonal pattern of deformation bands. Although basal  $\langle a \rangle$  slip may occur parallel to conjugate deformation bands/lamellae at low temperature (e.g., Gottardi and Tyssier, 2013), the major and secondary maxima would be normal to each other if the basal  $\langle a \rangle$  slip activates in the same way as in the high-temperature case. As a representative case for a quasi-orthogonal pattern, it has an opening angle of  $110^\circ \pm 10^\circ$  (PNG-06-034a in Figs 6a and 8b). The angle between the two trace sets in Figure 7a is  $\sim 70^\circ$  or  $110^\circ$  (rather than  $90^\circ$ ). For the case of PNG-06-024a,  $W_k=0.91$  (Fig. 6a) indicates that the prism  $\langle c \rangle$ -slip system on synthetic shear bands deviates slightly ( $\sim 4^\circ$ ) from the original C-foliation, with an opening angle of  $117^\circ \pm 10^\circ$ . This implies that the secondary maximum near the  $AP_1$ -normal belongs to the prism  $\langle c \rangle$ -slip system. For these reasons, it is more likely that the two maxima represent conjugate prism  $\langle c \rangle$ -slip sets at high temperature (Fig. 8a, b). Once the secondary maximum appears, the opening angle is  $\sim 110^\circ$  (and not  $0^\circ$ ) (PNG-06-034a, 10 in Fig. 6a; Fig. 8b).

The conjugate deformation bands in quartz grains are parallel not only to the conjugate  $\langle c \rangle$ -axis maxima but also to the preferred orientation of the long axes of the recrystallized quartz grains. In a similar way to the pattern shown in Figure 1, deformation partitioning on a microscale is likely responsible for this parallelism

between shear and  $ISA_1$  features.

#### 4.5 Type H-2

This pattern is associated with a pair of point maxima that appear asymmetrically on the sides of the  $AP_1$ , with the obtuse angle ( $\geq 110^\circ$ ) relative to the normal to  $AP_1$ . The front point maximum represents the prism  $\langle c \rangle$ -slip system on synthetic shear bands that deviate from the original orientation of the C-foliation. The predicted  $\sigma_1$  (or  $ISA_3$ ) is oriented  $55^\circ$  relative to the front maximum, implying a second stage of deformation caused by deformation partitioning. The two point maxima represent the second stage of deformation with the value of the vorticity number being  $0 < W_k < 0.94$ . The trail maximum may represent either  $\langle c \rangle$  slip on the S-foliation (for a trail maximum oriented  $35^\circ$ – $0^\circ$  relative to  $AP_1$ ) or  $\langle c \rangle$  slip on the antithetic shear bands (for a trail maximum oriented  $0^\circ$ – $35^\circ$  relative to  $AP_1$ ), depending on the degree of deformation partitioning (Tikoff and Teysier, 1994; Teysier et al., 1995; Fig. 6a).

#### 4.6 Type H-3

This pattern is associated with a pair of point maxima on  $AP_1$ , with an obtuse angle ( $\sim 110^\circ$ ) relative to the normal to  $AP_1$ . The pattern represents 100% deformation partitioning of the shear zone (Tikoff and Teysier, 1994; Teysier et al., 1995), implying that the original shear zone has been transformed into a “pure shear” zone. In a strict sense, the zone is not a shear zone, but a contractional zone, because the  $\langle c \rangle$ -slip system cannot function. The existence of this pattern confirms that the original shear zone was a quasi-simple shear, rather than a real simple shear zone, because the latter is characterized by a constant thickness with no shortening in the normal

direction.

The change in  $W_k$  is different from the change associated with reworked shear zones, in which each orogenic event could be associated with a different state of stress. The latter may be recognized by 1) an initial  $W_k \neq 0.94$ ; 2) an abrupt change in  $W_k$ ; 3) an inconsistent shear sense, associated with different tectonic events; and 4) reworked shear zones with a negative value of  $W_k$  (Simpson and De Paor, 1993).

## 5 The Opening Angle of Quartz <c>-Fabrics and Shear Bands

The opening angle of quartz <c>-axis fabrics, according to Kruhl (1996, 1998), may be used as a deformation thermometer in plane strain. This widely used thermometer is based on empirical data that show linear relationships between the opening angle and the deformation temperature in the range of 250 to 650°C (Morgan and Law, 2004). The opening angle is also sensitive to other parameters, such as water weakening, strain rate, and strain regime. Nonetheless, according to Law (2014), the deformation temperature can be estimated with an uncertainty of  $\pm 50^\circ\text{C}$ . For deformation at higher temperatures (650–1050°C), Faleiros et al. (2016) suggested a slightly different linear relationship. The change in the opening angle is attributed to a change in the mechanism of dynamic recrystallization.

It is important to note that low- and high-temperature quartz <c>-fabrics have different definitions for the opening angle. At low temperature, the opening angle is

the angle between the normals to two basal <a>-slip sets (Fig. 9a). At high temperature, this angle is measured between the two prism <c>-slip sets (Fig. 9b). Statistically, the most common opening angles in low- and high-temperature fabrics are  $70^\circ$  and  $110^\circ$ , respectively (Figs 7 and 9). Both angles are consistent with the MEM orientations. The abrupt change from  $70^\circ$  to  $110^\circ$  may reflect the transition from a basal <a>-slip to a prism <c>-slip at low temperature ( $\sim 400^\circ\text{C}$ ) and high temperature (600–650°C), respectively (Lister and Dornsiepen, 1982; Mainprice et al., 1986; Morgan and Law, 2004; Passchier and Trouw, 2005; Langille et al., 2010; Zhang et al., 2017). Establishing a linear correction between the two peaks is problematic owing to the abrupt change in the opening angle.

Quartz fabrics are sensitive to other factors in addition to temperature (Law 2014, and references therein). Therefore, thermometers that are based on a single criterion are problematic. The MEM criterion (Eq. 1), which considers the yielding point of the material based on multiple parameters (e.g., temperature, confining pressure, fluid pressure, and strain rate), may better account for the development of quartz <c>-axis fabrics and the associated opening angles.

## 6 Conclusions

Shear bands and deformation bands/lamellae nucleate in the orientations predicted by the MEM criterion, with  $\sigma_1$  (or  $\text{ISA}_3$ ) oriented  $55^\circ$  relative to the shear boundaries. In a steady state, spaced C- and penetrative S-foliation develop alternatively in a critical state of dynamic balance. The low-temperature basal <a>-slip and the high-temperature prism <c>-slip in quartz are both parallel to the shear boundaries, forming a single girdle in the direction normal to the  $\text{AP}_1$  and a unimodal maximum in the  $\text{AP}_1$  direction, respectively. Consequently, opening angles of  $\sim 70^\circ$  (for low-temperature fabrics) and  $\sim 110^\circ$  (for high-temperature fabrics) are produced. Non-steady deformation is most likely caused by deformation partitioning induced by changes in the stress state. In this case, synthetic shear bands progressively rotate from the orientation of the C-foliation until they reach an orientation of  $35^\circ$  relative to  $\text{AP}_1$ . The major opening angle for low-temperature fabrics is  $\sim 70^\circ$  and for high-temperature fabrics is  $\sim 110^\circ$ . As synthetic shear bands occur earlier than antithetic bands during deformation partitioning, opening angles may be smaller than  $70^\circ$  for low-temperature fabrics and larger than  $110^\circ$  for high-temperature fabrics.

## Acknowledgments

This research was funded by the National Natural Science Foundation of China (Grant No.41772207). Dr. Zhang Qing and Dr. Lamont Lan provided very helpful and insightful reviews that greatly improved the manuscript in conceptions and English expression.

Manuscript received Aug. 1, 2018  
accepted Dec. 20, 2018  
associate EIC YANG Jingsui

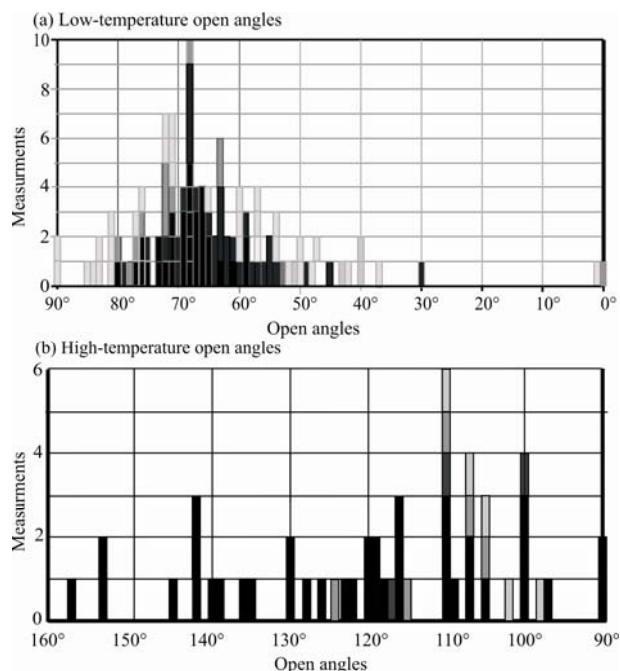


Fig. 9. Histograms of opening angles.

(a) Low-temperature quartz <c>-axis fabrics (black data from Law et al., 2013, dark from Law et al., 1994, gray from Little et al., 2013, and light gray from Faleiros et al., 2016); and (b) High-temperature quartz <c>-axis fabrics (black data from Faleiros et al., 2016, dark gray from Little et al., 2013, gray from Festa, 2014, and light gray from Cao et al., 2017).

edited by LIU Lian

## References

- Abbadi, M., Hahner, P., and Zeghloul, A., 2002. On the characteristic of Portevin-Le Chaterlier band in aluminum alloy 5182 under stress-controlled and strain-controlled tensile testing. *Materials Science & Engineering, A*, 337(1–2): 194–201.
- Ananthkrishna, G., 2007. Current theoretical approach to collective behavior of dislocation. *Physics Reports*, 440(4–6): 113–259.
- Becker, G.F., 1893. Finite homogeneous strain, flow and rupture of rocks. *Geological Society of America Bulletin*, 4(1): 13–90.
- Berthé, D., Choukroune, P., and Gapais, D., 1979. Orthogneiss mylonite and non-coaxial deformation of granites: the example of the South Armorican shear zone. *Journal of Structural Geology*, 1(1): 31–42.
- Bobyarchick, A.R., 1986. The eigenvalues of steady state flow in Mohr space. *Tectonophysics*, 122(1–2): 35–51.
- Cao, Sh.Y., Neubauer, F., Bernroider, M., Genser, J., Liu, J., and Friedl, G., 2017. Low-grade retrogression of a high-temperature metamorphic complex: Naxos, Cyclades, Greece. *GSA Bulletin*, 129(1–2): 93–117.
- Compton, R.R., 1980. Fabrics and strains in quartzites of a metamorphic core complex, Raft River Mountains, Utah. In: Crittenden, Jr. M.D., Coney, P.J., Davis, G.H. (Eds.), *Cordilleran Metamorphic Core Complexes*. Geological Society of America Memoir, 153: 271–279.
- Faleiros, F.M., Moraes, R., Pavan, M., and Campanha, G.A.C., 2016. A new calibration of the quartz c-axis fabric opening-angle deformation thermometer. *Tectonophysics*, 671: 173–182.
- Festa, V., 2014. The amount of pure and thinning in the Hercynian continental lower crust exposed in the Serre Massif (Calabria, southern Italy): an application of the vorticity analysis to quartz c-axis fabrics. *Italian Journal of Geoscience*, 133(2): 214–222.
- Gillam, B.G., Little, T.A., Smith, E., and Toy, V.G., 2014. Reprint of extensional shear band development on the outer margin of the Alpine mylonite zone, Tartare stream, Southern Alps, New Zealand. *Journal of Structural Geology*, 64: 115–134.
- Gomez-Rivas, E., 2008. Localización de deformación en medios dúctiles y anisótropos: 163 estudio de campo, experimental y numérico. Tesis doctoral, Universitat Autònoma de Barcelona. <http://www.tesisenxarxa.net/TDX-1120108-151236/>
- Gomez-Rivas, E., and Griera, A., 2012. Shear fractures in anisotropic ductile materials: An experimental approach. *Journal of Structural Geology*, 34: 61–76.
- Gottardi, R., and Teyssier, C., 2013. Thermomechanics of an extensional shear zone, Rift River metamorphic core complex, NW Utah. *Journal of Structural Geology*, 53: 54–69.
- Grasemann, B., Stüwe, K., and Vannay, J.C., 2003. Sense and non-sense of shear in flanking structure. *Journal of Structural Geology*, 25(1): 19–34.
- Heilbronner, R., and Tullis, J., 2006. Evolution of c-axis pole figures and grain size during dynamic recrystallization: results from experimentally sheared quartzite. *Journal of Geophysical Research*, 111(B10).
- Hubert-Ferrari, A., King, G., Manighetti, I., Aomijo, R., Meyer, B., and Tapponnier, P., 2003. Long-term elasticity in the continental lithosphere: modeling the Aden Ridge propagation and the Anatolian extrusion process. *Geophysical Journal International*, 153(1): 111–132.
- Kruhl, J.H., 1996. Prism- and basal-plane parallel subgrain boundaries in quartz; a microstructural geothermobarometer. *Journal of Structural Geology*, 14(5): 581–589.
- Kruhl, J.H., 1998. Reply: Prism- and basal-plane parallel subgrain boundaries in quartz; a microstructural geothermobarometer. *Journal of Structural Geology*, 16: 142–146.
- Kurd, G.A., and Northrup, C.J., 2008. Structural analysis of mylonitic rocks in the Cougar Creek Complex, Oregon-Idaho using the porphyroclast hyperbolic distribution method, and potential use of SC<sup>2</sup>-type extensional shear bands as quantitative vorticity indicators. *Journal of Structural Geology*, 30(8): 1005–1012.
- Langille, J.M., Jessup, M.J., Cottle, J.M., Newell, D., and Seward, G., 2010. Kinematic evolution of the Ama Drime Detachment: insights into orogen-parallel extension and exhumation of the Ama Drime Massif, Tibet-Nepal. *Journal of Structural Geology*, 32(7): 900–919.
- Law, R.D., 1986. Relationships between strain and quartz crystallographic fabrics in the Roche Maurice quartzites of Plougastel, Western Brittany. *Journal of Structural Geology*, 8(5): 493–515.
- Law, R.D., 2014. Deformation thermometry based on quartz c-axis fabrics and recrystallization microstructures: A review. *Journal of Structural Geology*, 66: 129–161.
- Law, R.D., Knipe, R.J., and Dayan, H., 1984. Strain path partitioning within thrust sheets: microstructural and petrofabric evidence from the Moine thrust zone at Loch Eriboll, NW Scotland. *Journal of Structural Geology*, 6(5): 477–497.
- Law, R.D., Miller, E.L., Little, T.A., and Lee, J., 1994. Extensional origin of ductile fabrics in the Schist Belt, Central Brooks Range, Alaska—II. Microstructural and petrofabric evidence. *Journal of Structural Geology*, 16(7): 919–940.
- Law, R.D., Stahr, D.W., Francis, M.K., Ashley, K. T., Grasemann, B., and Ahmad, T., 2013. Deformation temperatures and flow vorticities near the base of the Greater Himalayan Series, Sutlej Valley and Shimla Klippe, NW India. *Journal of Structural Geology*, 54: 21–53.
- Lister, G.S., 1977. Discussion: crossed-girdle c-axis fabrics in quartzites plastically deformed by plane strain and progressive simple shear. *Tectonophysics*, 39(1–3): 51–54.
- Lister, G.S., and Dornsiepen, U.F., 1982. Fabric transitions in the Saxony granulite terrain. *Journal of Structural Geology*, 4(1): 81–92.
- Lister, G.S., and Hobbs, B.E., 1980. The simulation of fabric development during plastic deformation and its application to quartzite: the influence of deformation history. *Journal of Structural Geology*, 2(3): 355–370.
- Lister, G.S., Paterson, M.S., and Hobbs, B.E., 1978. The simulation of fabric development in plastic deformation and its application to quartzite: the model. *Tectonophysics*, 45(2–3): 107–158.
- Lister, T.A., and Snoko, A.W., 1984. S-C mylonites. *Journal of Structural Geology*, 6(6): 617–638.
- Little, T.A., Hacker, B.R., Brownlee, S.J., and Seward, G., 2013. Microstructures and quartz lattice-preferred orientations in the eclogite-bearing migmatitic gneisses of the D'Entrecasteaux Islands, Papua New Guinea. *Geochemistry, Geophysics, Geosystems*, 14(6): 2030–2062.
- Little, T.A., Hacker, B.R., Gordon, S.M., Baldwin, S.L., Fitzgerald, P.G., Ellis, S., and Korchinski, M., 2011. Diapiric exhumation of Earth's youngest (UHP) eclogites in the gneiss domes of the D'Entrecasteaux Islands, Papua New Guinea. *Tectonophysics*, 510(1–2): 39–68.
- Mainprice, D., Bouchez, J.L., Blumenfeld, P., and Tubià, J. M., 1986. Dominant c slip in naturally deformed quartz: implications for dramatic plastic softening at high temperature. *Geology*, 14(10): 819–822.
- Morgan, S.S., and Law, R.D., 2004. Unusual transition in quartzite dislocation creep regimes and crystal slip systems in the aureole of the Eureka Valley-Joshua Flat-Beer Creek pluton, California: a case for anhydrous conditions created by decarbonation reactions. *Tectonophysics*, 384(1–4): 209–231.
- Passchier, C.W., 1986. Flow in natural shear zones—the consequences of spinning flow regimes. *Earth and Planetary Science Letters*, 77(1): 70–80.
- Passchier, C.W., and Trouw R.A., 2005. *Microtectonics*, Springer-Verlag, Heidelberg, Berlin.
- Platt, P., and Vissers, R.L.M., 1980. Extensional structures in anisotropic rocks. *Journal of Structural Geology*, 2(4): 397–410.
- Price, J.P., 1985. Preferred orientations in quartzites. In: Wenk, H.R. (ed.), *Preferred Orientations in Deformation Metals and Rocks: An Introduction to Modern Texture Analysis*.

- Academic Press, Orlando, 385–406.
- Ramsay, J.G., 1980. Shear zone geometry: a review. *Journal of Structural Geology*, 2(1–2): 83–99.
- Sarkarinejad, K., Keshavarz, S., and Faghih, A., 2015. Kinematics of the Sirjan mylonite nappe, Zagros Orogenic Belt: insights from strain and vorticity analyses. *Journal of Geosciences*, 60(3): 189–202.
- Schmid, S.M., and Casey, M., 1986. Complete fabric analysis of some commonly observed quartz c-axis patterns. In: Hobbs, E. and Heard, H.C. (eds.) *Mineral and Rock Deformation Laboratory Studies: The Paterson Volume*. American Geophysical Union, *Geophysical Monograph*, 36: 263–286.
- Simpson, C., and De Paor, D.G., 1993. Strain and kinematic analysis in general shear zones. *Journal of Structural Geology*, 15(1): 1–20.
- Sullivan, W.A., 2009. Kinematic significance of L tectonites in the footwall of a major terran-thrust fault Klamath Mountains, California, USA. *Journal of Structural Geology*, 31(10): 1197–1211.
- Sullivan, W.A., and Beane, R.J., 2010. Asymmetrical quartz crystallographic fabrics formed during constrictional deformation. *Journal of Structural Geology*, 32(10): 1430–1443.
- Teyssier, C., Tikoff, B., and Markley, M., 1995. Oblique plate motion and continental tectonics. *Geology*, 23(5): 447–450.
- Tikoff, B., and Fossen, H., 1995. The limitations of three-dimensional kinematic vorticity analysis. *Journal of Structural Geology*, 17(12): 1771–1784.
- Tikoff, B., and Teyssier, C., 1994. Strain modeling of displacement field partitioning in transpressional orogens. *Journal of Structural Geology*, 16(11), 1575–1588.
- Tullis, J., 1977. Preferred orientation of quartz produced by slip during plane strain. *Tectonophysics*, 39(1–3): 87–102.
- Wallis, S.R., 1995. Vorticity analysis and recognition of ductile extension in the Sanbagawa belt, SW Japan. *Journal of Structural Geology*, 17(8): 1077–1093.
- Weijermars, R., 1991. The role of stress in ductile deformation. *Journal of Structural Geology*, 13(9): 1061–1078.
- Weijermars, R., 1998. Taylor-mill analogues for patterns of flow and deformation in rocks. *Journal of Structural Geology*, 20(1): 77–92.
- White, S.H., 1979. Large strain deformation: Report on a tectonic studies group discussing meeting held at Imperial College, London on 14 November 1997. *Journal of Structural Geology*, 1(4): 333–339.
- Xypolias, P., 2010. Vorticity analysis in shear zones: A new review of methods and applications. *Journal of Structural Geology*, 32(12): 2027–2092.
- Zhang, B., Yin, C.Y., Zhang, J.J., Wang, J.M., Zhong, D.L., Wang, Y., Lai, Q.Z., Yue, Y.H., and Zhou, Q.Y., 2017. Midcrustal shearing and doming in a Cenozoic compressive setting along the Ailao Shan-Red River shear zone. *Geochemistry, Geophysics, Geosystem*, 18(1): 400–433.
- Zheng, Y.D., Wang, T., and Zhang, J.J., 2009. Comment on “Structural analysis of mylonitic rocks in the Cougar Creek Complex, Oregon-Idaho using the porphyroclast hyperbolic distribution method, and potential use of SC'-type extensional shear bands as quantitative vorticity indicators”. *Journal of Structural Geology*, 31: 541–543.
- Zheng, Y.D., Wang, T., Ma, M., and Davis, G.A., 2004. Maximum effective moment criterion and the origin of low-angle normal faults. *Journal of structural Geology*, 26(2): 271–285.
- Zheng, Y.D., Zhang, J.J., and Wang T., 2014. Interpretation of the experimental data provided by Gomez-Rivas and Grier (2012) in terms of the MEM-criterion. *Science China Earth Sciences*, 57(11): 2819–2824.
- Zheng, Y.D., Zhang, J.J., and Wang, T., 2011. Puzzles and the maximum-effective-moment (MEM) criterion in structural geology. *Journal of structural Geology*, 33(9): 1394–1405.
- Zheng, Y.D., Zhang, Q., and Hou, Q.L., 2015. Deformation localization: a review on the Maximum-Effective-Moment (MEM) Criterion. *Acta Geologica Sinica (English Edition)*, 89(4): 1133–1152.

#### About the first author



ZHENG Yadong, male, born in January 1936, Professor in Structural geology and Tectonics, School of Earth and Space Sciences, Peking University, Beijing 100871, China.

#### About the corresponding author



ZHANG Bo, Associated professor in Structural geology and Tectonics, School of Earth and Space Sciences, Peking University, Beijing 100871, China. Mainly engaged in structural geology and micro-structural geology. Main aspects of interest are based on macro-microscopic structural analysis, to reveal the tectonic geometry, kinematics, tectonic geomorphology and dynamic process of the intracontinental deformation and orogenic belts. The study area is mainly in the Tibet Plateau, western Yunnan and Southeast Asia.